ORIGINAL ARTICLE

gebiology WILEY

White and green rust chimneys accumulate RNA in a ferruginous chemical garden

Vanessa Helmbrecht[1] [ORCID] | Maximilian Weingart[2] | Frieder Klein[3] | Dieter Braun[2] | William D. Orsi[1,4]

[1]Department for Geo- and Environmental Sciences, Palaeontology & Geobiology, Ludwig-Maximilians-Universität, Munich, Germany

[2]Systems Biophysics, Faculty of Physics, Ludwig-Maximilians-Universität, Munich, Germany

[3]Department of Marine Chemistry and Geochemistry, Woods Hole Oceanographic Institution, Woods Hole, Massachusetts, USA

[4]GeoBio-Center[LMU], Ludwig-Maximilians-Universität München, Munich, Germany

Correspondence
William D. Orsi, Department for Geo- and Environmental Sciences, Palaeontology & Geobiology, Ludwig-Maximilians-Universität, 80333 Munich, Germany.
Email: w.orsi@lrz.uni-muenchen.de

Abstract

Mechanisms of nucleic acid accumulation were likely critical to life's emergence in the ferruginous oceans of the early Earth. How exactly prebiotic geological settings accumulated nucleic acids from dilute aqueous solutions, is poorly understood. As a possible solution to this concentration problem, we simulated the conditions of prebiotic low-temperature alkaline hydrothermal vents in co-precipitation experiments to investigate the potential of ferruginous chemical gardens to accumulate nucleic acids via sorption. The injection of an alkaline solution into an artificial ferruginous solution under anoxic conditions ($O_2 < 0.01\%$ of present atmospheric levels) and at ambient temperatures, caused the precipitation of amakinite ("white rust"), which quickly converted to chloride-containing fougerite ("green rust"). RNA was only extractable from the ferruginous solution in the presence of a phosphate buffer, suggesting RNA in solution was bound to Fe^{2+} ions. During chimney formation, this iron-bound RNA rapidly accumulated in the white and green rust chimney structure from the surrounding ferruginous solution at the fastest rates in the initial white rust phase and correspondingly slower rates in the following green rust phase. This represents a new mechanism for nucleic acid accumulation in the ferruginous oceans of the early Earth, in addition to wet-dry cycles and may have helped to concentrate RNA in a dilute prebiotic ocean.

KEYWORDS
alkaline vents, emergence of life, ferruginous, green rust, RNA accumulation, white rust

1 | INTRODUCTION

There are many theories on a possible emergence of life at alkaline hydrothermal vents (AHVs) on Earth. The "RNA world" theory (Gilbert, 1986), and the "metabolism first" theory at AHVs (Martin et al., 2008) feature prominently in the discussion about the emergence of life and are now considered to be not necessarily mutually exclusive (Preiner et al., 2020). A key unknown in the emergence of

life is, how nucleic acids could overcome the large dilution factor of the prebiotic oceans, which has been referred to as the "concentration problem" (De Duve, 1991). It has been proposed, that AHV chimneys could accumulate nucleic acids including RNA during the RNA world (Martin & Russell, 2003). In this scenario, AHV chimneys provide an alternative RNA concentration site to the wet-dry cycles that have been proposed for 'warm little ponds' (Damer & Deamer, 2020; Darwin, 1871; Pearce et al., 2017).

—WILEY

Few studies so far have shown evidence for compatibility of nucleic acids within an AHV environment (Altair et al., 2021; Baaske et al., 2007; Burcar et al., 2015; Mast & Braun, 2010) but RNA accumulation dynamics at an AHV are poorly understood. Some studies that focus on the adsorption of RNA test mineral surfaces like iron sulfides (Mizuuchi et al., 2019) or clay minerals (Pedreira-Segade et al., 2016).

Compared to modern oceans, prebiotic oceans of the Hadean and Archean were likely more acidic and ferruginous, that is, anoxic conditions with high concentrations of dissolved iron (Poulton & Canfield, 2011). As soon as liquid water oceans were present on Earth ~4.4 Ga ago (Heller et al., 2021; Mojzsis et al., 2001), water would have interacted with ultramafic to mafic seafloor rocks, resulting in widespread hydrothermal alteration, including serpentinization across the Hadean seafloor (Figure 1a; Rouillard et al., 2018; White et al., 2020). The pH of the emanating fluids is increasingly alkaline pH with decreasing temperatures (Klein et al., 2013; Rouillard et al., 2018).

The likely ferruginous conditions of the prebiotic oceans suggest the existence of a different kind of chimney at AHVs on early Earth (Figure 1b) compared to the white calcium carbonate and brucite smokers seen at Lost City today (Kelley et al., 2001), and other serpentinization hosted systems (Charlou et al., 1998). However assuming a circumneutral pH (~6.6) of the ocean around 4.0 Ga, it has been proposed that carbonates and brucite could have existed as well (Krissansen-Totton et al., 2018). Previous studies argue for the presence of "green rust" as an important mineral in the emergence of life at AHVs, since green rust can form inorganic membranes to maintain disequilibria between the acidic ocean and the alkaline interior of the vents (Altair et al., 2021; Arrhenius, 2003; Barge et al., 2015; Duval et al., 2019; Halevy et al., 2017; Russell, 2018). The highly redox-reactive mineral green rust is a ferrous-ferric oxyhydroxide also known as fougerite (Bernal et al., 1959; Halevy et al., 2017; Trolard et al., 2007). Amakinite or "white rust", the rare ferrous analogue of brucite, is the precursor phase of fougerite and was detected in

the basement rocks below the Lost City hydrothermal field (Beard et al., 2009; Trolard et al., 2022).

Despite acknowledging the minerals' significance in an emergence of life context, experimental evidence for alkaline vents made out of white and green rust chimneys, is scarce (Altair et al., 2021). Moreover, their capability to accumulate nucleic acids to avoid dilution in a prebiotic ocean, to our knowledge, has not been tested. Therefore, we tested the hypothesis that AHV chimneys can concentrate RNA (Martin & Russell, 2003), offering a potential solution to the 'concentration problem' (De Duve, 1991).

We created alkaline vents under ferruginous conditions thought to a defining feature of the prebiotic oceans (Poulton & Canfield, 2011) under O_2 concentrations less than 0.01% of present atmospheric levels. Within these ferruginous chemical gardens, chimney structures composed of the iron-containing hydroxide white rust and the layered double hydroxide green rust form across strong pH gradients. We show that the chimneys accumulate RNA from the surrounding ferruginous solution at rates that depend on the formation of white and green rust. In a prebiotic ocean on early Earth, this process may have helped to overcome dilution of the RNA to very low concentrations, supporting the hypothesis that AHV chimneys can concentrate RNA in a ferruginous environment (Martin & Russell, 2003).

2 | METHODS

2.1 | Experimental setup

Similar to previous AHV experiments (Altair et al., 2021; Barge et al., 2015), our experimental setup was designed to mimic ferruginous early Earth conditions (Figure 1a). Five AHV experimental replicates were performed in an anaerobic chamber (MBRAUN Labstar) containing a N_2 atmosphere to maintain anoxic conditions. Oxygen
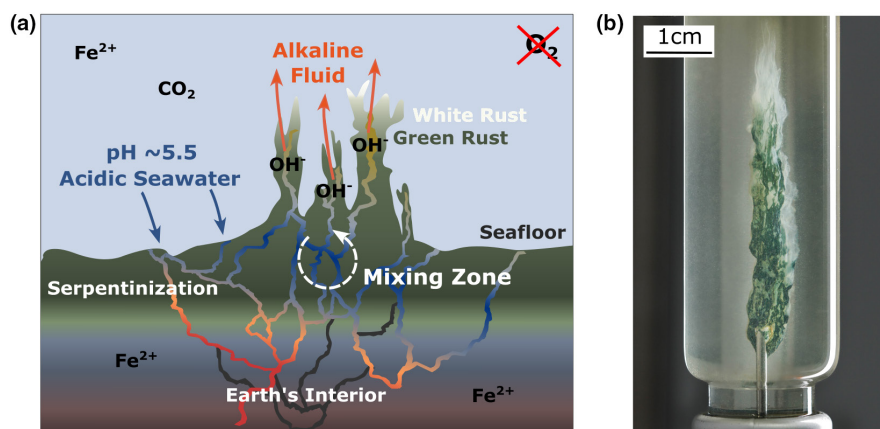
FIGURE 1 Alkaline vents and the emergence of life in a ferruginous environment. (a) Schematic drawing of the seafloor conditions during the ferruginous oceans of the Hadean and Archean. The pH of the seawater was ~5.5. Acidic seawater gets reduced by Fe^{2+}-containing rocks (e.g., olivine) in the Earth's interior, releasing OH^- via serpentinization, fueling the formation of alkaline vents. (b) White and green rust chimney formed in a 20 mL vial through the mixing of an alkaline fluid with a ferruginous solution. Injection rate: 5 mL/h.

values were continuously monitored inside the anaerobic chamber using two digital sensors. They were constantly below <0.01% of present atmospheric levels. Experiments were carried out at room temperature (25°C) as it seems likely that low-temperature systems were widespread in off-axis environments.

Our experimental setup was similar to those used in previous studies where an alkaline solution representing the hydrothermal fluid is slowly pumped into a ferruginous solution representing the ocean (Barge et al., 2015, 2020; Burcar et al., 2015; White et al., 2015; Figure S1). We used an inverted 125 mL glass vial with the bottom cut off to hold the ferruginous solution. The vial was sealed with a rubber stopper (Figure S1) and a pipette tip was inserted through the crimp-seal and connected to a polymer tube on the outside (bottom) of the inverted flask, which was connected to a syringe 10 mL Luer-lock plastic syringe (B Braun) filled with alkaline NaOH (Carl Roth) solution. The polymer tubing was connected to the syringe via a Sterican® hypodermic-needle (B Braun, 1.20×50 mm, 18 G×2). The syringe was mounted on a single-syringe pump (Cole Parmer, Model 100 78-9100C), that was vertically oriented to ensure a constant flow rate of alkaline fluid from the syringe into the simulated iron ocean. Horizontal orientation of the syringe and syringe pump was found to result in less stable chimneys, because the required longer tubing length caused introduction of gas bubbles that disrupted chimney growth. Vertical orientation of the syringe and syringe pump, and the shorter tubing length greatly ameliorated this problem.

A 100 mL solution with 0.2 M $FeCl_2$*$4H_2O$ (Sigma-Aldrich) and MilliQ water resulted in ferruginous and acidic (pH 3) conditions. The alkaline (pH 13) hydrothermal solution consisted of 0.2 M NaOH (Carl Roth) dissolved in MilliQ water. All solutions were prepared inside the anaerobic chamber to ensure anoxic conditions and reduce the presence of dissolved O_2 in the solutions. The alkaline NaOH solution was injected into the ferruginous solution at a rate of 3.7 mL/h. The pH of the ferruginous solution was monitored over the duration of the experiment using a pH meter. After ~2 h and injection of 7 mL NaOH, chimney growth ceased. A total of 12 mg dry-powdered total RNA from the yeast *Saccharomyces cerevisiae* (Sigma-Aldrich, catalog number 10109223001) was dissolved in the ferruginous solution (before the injection started) to achieve a mean starting concentration (+/− standard error of the mean) at $t(_0)$ of (3.96 +/− 0.54) ng/ μL in all five experimental replicates (Table S1). The powder was weighed using a high sensitivity scale with an analytical variation of ±1 mg. The starting concentration of RNA slightly varied because of the uneven dissolution of the RNA powder.

2.2 | RNA sampling, extraction and quantification

Inside the anaerobic chamber, 1 mL samples of the ferruginous solution were taken with a pipettor at set time intervals as the chimney grew. At the end of the experiment, the chimney was dried in the anaerobic chamber for 24 h and frozen for subsequent RNA extraction (see below). All RNA extractions from the ferruginous solution and the green rust chimneys were performed in a laminar flow clean bench equipped with a high-efficiency particulate air filter. The clean bench is a dedicated bench for RNA only with its own dedicated set of pipettors, racks and tubes, where no DNA samples or PCR products are introduced (Orsi et al., 2022). This helps to maintain a relatively low level of RNA and DNA contamination from aerosols as well as DNA contamination from PCR products. All surfaces are sterilized with UV prior and after sample processing and all surfaces are wiped down with RNAseZap to remove any potential contaminating microbes or aerosolized RNA.

During the experiment within the anaerobic chamber, the ferruginous solution was sampled at a consistent frequency every 10 min in all five experimental replicates, and additionally every minute in the first 10 min in experimental replicates 3, 4 and 5 (Table S3) to capture a high temporal resolution from the initial period of chimney formation where the most rapid RNA depletion in the ferruginous solution simulant was observed. The liquid samples were immediately transferred to RNA/DNA clean 2 mL Eppendorf tubes that were frozen at −20°C. RNA was extracted by adding 1 mL of acidic (pH: 4) trizol (MP Biomedicals) and 1 M Na_2HPO_4 (Sigma-Aldrich) powder. The addition of the phosphate buffer was used to reduce RNA adsorption to iron particles in the ferruginous solution, which is a well-known feature of iron minerals that can reduce nucleic acid extraction efficiencies (Muto et al., 2017). The solutions were mixed by vortexing for 10 s and centrifuged for 10 min at 4°C (to increase RNA preservation and strengthen the trizol phase separation) at 13,000 rpm. The supernatant (containing the dissolved RNA) was transferred via pipetting to a new 2 mL RNA/DNA free tube. An equal volume of ≥99.5% isopropanol (Carl Roth) and 3 μL glycogen (Carl Roth) as a carrier were added to help precipitate the relatively low concentrations of RNA. Precipitation was done overnight at −20°C. RNA was pelleted by centrifugation (5 min at 4°C, 13,000 rpm). The pellets were air dried in an RNA-dedicated laminar flow hood (see above) with HEPA filtered air to reduce contamination. To remove residual salts, the pellets were washed with 500 μL of 70% molecular biology grade ethanol (Carl Roth) centrifuged for 5 min and air dried in the laminar flow clean hood. After air drying, the RNA pellets were resuspended in RNAse free diethyl pyrocarbonate (DEPC) treated water (Carl Roth) and vortexed for 30 s to resuspend the RNA. Quantification was done with an Invitrogen Qubit 3 Fluorometer and the micro–RNA kit.

After the AHV experiment, the ferruginous solution was drained with a pipette and the chimney was dried out for 1 day inside the anaerobic chamber. The dried chimney was weighed and placed in a sterile RNA free 2 mL screw cap microtube (MP Biomedicals, Lysing Matrix E) containing 0.5 mL of differently sized silica beads. The silica beads were added to the RNA extraction step to physically disrupt the chimney structure during beating in order to enhance RNA retrieval during the extraction. RNA extractions were optimized using 1 mL of acidic (pH: 4) Phenol:Chloroform:Isoamyl alcohol ('trizol'). To desorb the RNA off of the green rust, 1 M Na_2HPO_4 was added since the addition of a phosphate buffer assists in desorbing RNA off of mineral surfaces (Muto et al., 2017). Chimney samples were homogenized in the presence of the acidic trizol and phosphate buffer in the Lysing

Matrix E tubes, using a Fastprep-24 5G (MP Biomedicals) at a speed of 6.0 m/s for 40 s. The samples were centrifuged for 10 min at 4°C and 13,000 rpm and the upper aqueous phase (containing the RNA) was transferred to new 2 mL Eppendorf tubes. The RNA was precipitated by adding an equal volume of isopropanol and 3 μL glycogen each. All samples were frozen overnight at −20°C. Pelleting, washing and measuring the RNA was done as described in the previous paragraph.

2.3 | Raman spectroscopy

The dry green rust chimneys were stored under an N_2 atmosphere to minimize oxidation prior to the analysis with the Raman spectrometer (HORIBA Jobin Yvon XploRA, Mineralogical State Collection Munich). For data acquisition, the chimneys were taken out of the anaerobic chamber. Exposure to air was less than 2 min until the start of the first Raman measurement. After 30 min, the chimney was completely oxidized and no green rust was detectable anymore. The settings of the scans were as follows: spectral range from 50 to 4000 cm^{-1}, 10 s acquisition time, 2 accumulations, 300 μm confocal hole and 100 μm slit, 1800 grooves/mm grating and a filter with 10 to 25% optical density of the incoming laser to avoid laser-induced oxidation of the chimney. A green laser with a wavelength of 532 nm, the ×100 long working distance (LWD) objective (0.80 numerical aperture) were used for all measurements and the Labspec 6 software was used to process the acquired spectra. We used an in-house reference Raman database MSC-RD (Mineralogical State Collection Raman Database, Drozdovskiy et al., 2020), the KnowItAll database (Horiba Edition, now John Wiley & Sons) and the database from the RRUFF™ Project (Lafuente et al., 2015). The instrument was calibrated with a silicon wafer (520.7 cm^{-1}) daily and immediately before the measurements took place.

2.4 | Scanning electron microscopy

We used a Phenom XL G2 scanning electron microscope (SEM) to further characterize the mineralogy of chimneys under vacuum. The dry chimneys were stored under an N_2 atmosphere until measurements started. Air exposure during transfer to the vacuum chamber of the SEM was limited to 30 s maximum. All measurements were carried out using an acceleration voltage of 10 kV, a beam current of 1 μA-pA, a vacuum pressure of 0.10 Pa and a beam diameter of 0.005 to 1 μm. For imaging, secondary electrons (SE) and backscattered electrons (BSE) were used. Elemental analysis of the green rust chimneys was carried out with the electron dispersive X-ray spectroscopy detector (EDX).

2.5 | Imaging, processing, quantifying chimney growth

Images of chimneys were taken with a Sony Alpha a6000 mirrorless camera and a 90 mm Sony macro lens. The images were processed

using the Adobe Lightroom and Photoshop software packages and the height of the chimney was determined in Adobe Photoshop with a ruler. Timelapse videos were taken with the Sony Alpha a6000 as well. The camera took an image of the chimney every 1–2 s during growth. The raw timelapse videos from the camera were sped up x20 times in post-production.

## 3 | RESULTS

3.1 | Chimney morphology

Five different AHV experiments were carried out in an anaerobic chamber in a N_2 atmosphere. During chimney growth, the pH was constantly monitored and it remained at pH 3 for the entire duration of the experiment. In all five experimental replicates, the injection of the alkaline fluid resulted in the formation of chimney structures within 90 min. These structures resemble "chemical gardens" that have been found to form in AHV models across steep pH gradients (Altair et al., 2021). The average height of the chimneys (+/− standard error of mean) was (3.7 +/− 0.2) cm. The average width was (0.6 +/− 0.2) cm. The fastest growth rates were observed in the first 10 min of the five experimental replicates (Figure 3b). The raw RNA data for all five experiments is displayed in Table S1. After the initial growth phase, which ended after 10 min, vertical chimney growth slowed down significantly, after which horizontal growth of small mm-sized branches was observed. No more vertical growth was noted after 90 min. Growth of additional chimney extensions was detected only in two out of five experiments after 90 min of chimney growth.

A reproducible color transition pattern was observed during all experiments, whereby the base of the chimney would change from being translucent or white color to a green color in 5 min only. Then, as the chimneys grew, the green color gradually moved upwards towards the top replacing the white color by the end of the experiment. After a few minutes, the surface of the green precipitate would break and a new chimney structure would grow vertically on top of the green structure (Videos S1–S3). These new structures also appeared first as a white film, which turned green also within 4 to 5 min of exposure to the ferruginous solution. This process of constant ruptures, re-precipitation and color transition continued, until the chimneys reached their maximum heights. A visualization of the phase transition from the white film to green colored chimney structure is presented in Figure 3e and in Videos S1–S3.

3.2 | Green rust identification

The fully grown chimney shows a complex morphology on a macroscopic and a microscopic scale. SEM images show that the chimney is composed of a thin inorganic 'membrane' of euhedral hexagonal plate-shaped crystals (Figure 2a) that are similar in size

(a)

(b)

(c)
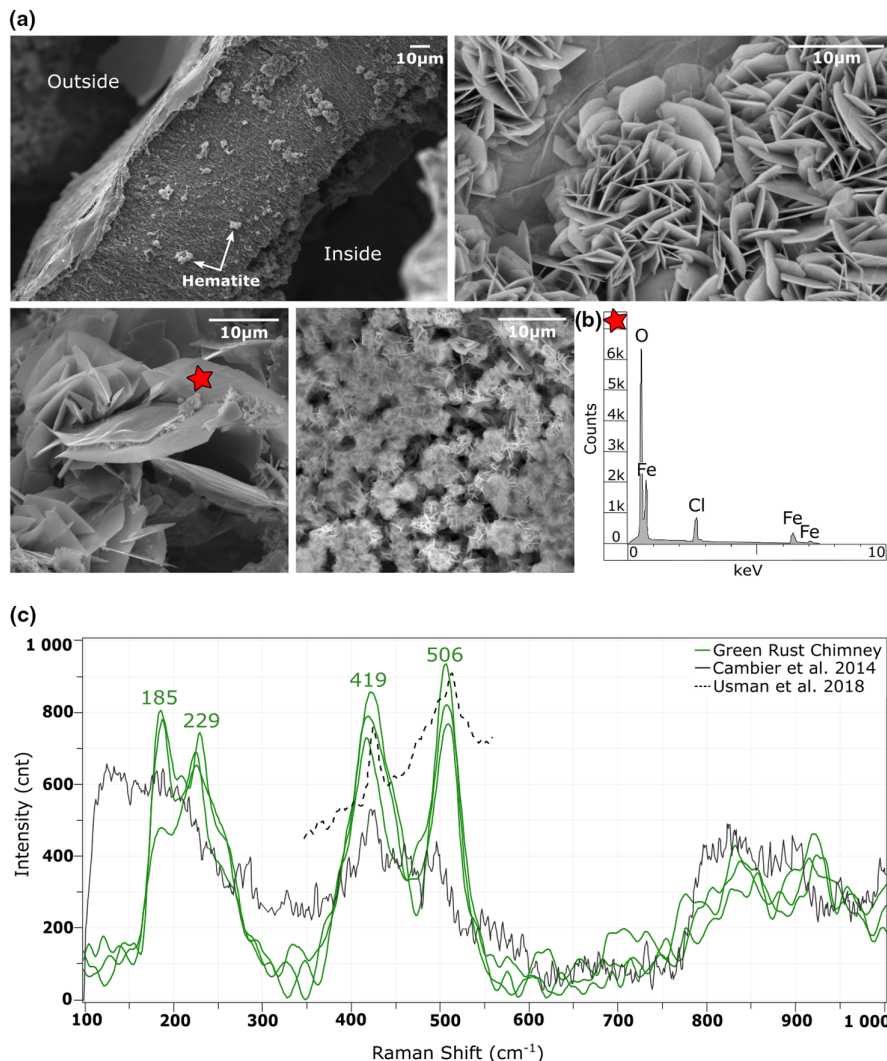
FIGURE 2 Dried chimney structures are composed primarily of green rust. (a) BSE images of a dried green rust chimney. The first image shows a chimney wall with a thickness of approx. 80 to 90 μm. Hematite globules are located on top of the green rust. The other BSE images show different magnifications of hexagonal platy green rust crystals. Contamination with oxygen during the transfer to the vacuum chamber was limited to max. 1 min transfer time. (b) EDX spectrum with the elemental composition of the chimney in the marked region (red star). Acquisition settings were 30 s time, 10 kV acceleration voltage and 0.10 Pa vacuum pressure. (c) Raman spectra of a green rust chimney made with 0.2 M NaOH and 0.2 M $FeCl_2{*}4H_2O$. The significant Raman bands for green rust identification are at 427 and 518 cm^{-1} (Usman et al., 2018). Other mineral peaks except green rust peaks were removed from the Cambier et al. (2014) spectrum for simplification.

and shape to green rust (Duval et al., 2019; Usman et al., 2018). Crystals formed aggregates, with individual crystals ranging in diameter from <1 μm to approximately 20 μm. The chimneys contain an inorganic membrane with a width between 80 to 90 μm (Figure 2a). SEM images also revealed a high internal pore space and surface area with nanopores (<1 μm) and channels in the chimney structure (Figure 2a).

Raman spectra of a dried chimney suggests that it is mainly composed of green rust (Figure 2c). This evidence is based on the characteristic Raman bands at 427 and 518 cm^{-1}, that are considered diagnostic for green rust identification (Trolard et al., 2007; Usman et al., 2018). The EDX spectrum highlights the elemental composition of the chimneys, which is consistent with chloride-bearing green rust (Figure 2b). Chloride green rust has a chemical composition of ~$[Fe_3{}^{2+}Fe^{3+}(OH)_8]^+[Cl{\cdot}2H_2O]^-$ (Arrhenius, 2003; Barge et al., 2015; Russell et al., 2013). When left exposed to air for more than 20 min, the chimneys changed color quickly from dark green to an ochre color indicating oxidation of iron. Based on SEM and Raman analyses, these oxidation products were identified as hematite (Figure 2a; Figure S2).

3.3 | RNA depletion from the ferruginous solution during chimney growth

A rapid decrease of RNA in the ferruginous solution was observed primarily during initial stages of chimney growth in all five experimental replicates (Figure 3b). RNA starting concentrations ranged from 1.99 to 5.27 ng/μL, because the powder containing the yeast RNA did not dissolve completely. We presume the powder might contain additional water insoluble components (for example lipids) to RNA that are unknown and not listed by the manufacturer. Nevertheless, the standard error (0.54) of the average starting concentration of 3.96 ng/μL is only 14% (Table S1). No matter the starting concentration, the same depletion trend was observed across all five experimental replicates. Figure 3d highlights the first 10 min of RNA depletion in experimental replicates 3, 4 and 5 (error bars show standard error of the means). RNA concentration values are listed in the Table S3. Figure 3d shows that the fastest RNA depletion rate in solution takes place in the first 4 min from an average of 4.82 ± 0.30 ng/μL of RNA to 1.02 ± 0.32 ng/μL of RNA, which coincides with the white rust phase of the chimney. In this time,
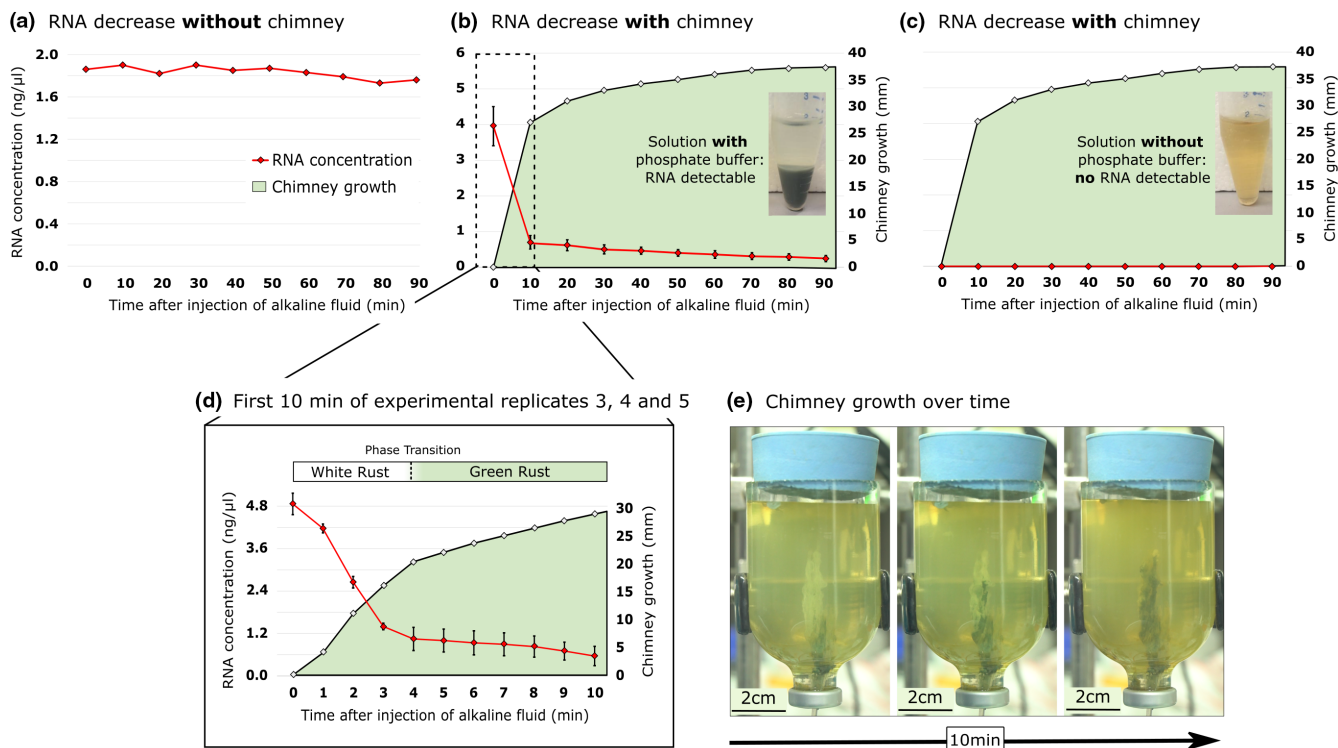
FIGURE 3 RNA is depleted from the ferruginous solution only in the presence of chimneys. RNA extractions were performed by adding a phosphate buffer ($1\,M\,Na_2HPO_4$) to desorb the RNA from the iron in the solution. (a) Rate of RNA depletion in the ferruginous solution without a chimney (control experiment). (b) Rate of RNA depletion from the solution with a chimney. Error bars show the standard error of the mean across five experimental replicates. RNA extractions were performed with a phosphate buffer, which precipitated together with the iron at the bottom of the sample tubes. The RNA remained in solution. (c) RNA extractions without a phosphate buffer. The same five samples as in (b) were used. Without phosphates, no RNA was extractable because the RNA was still bound to the iron in solution. This highlights the positive effect of adding phosphate to the RNA extraction protocol. (d) First 10 min of experimental replicates 3, 4 and 5. Error bars show the standard error of the mean. (e) White $Fe(OH)_2$ oxidation to green rust in contact with the ferruginous solution. RNA concentration values in Tables S1 and S3.

the three replicate chimneys show an average growth from 0 to 22.33 mm. After 4 min, RNA depletion rates slowed down significantly and the concentrations only dropped from 1.02 ± 0.32 ng/μL to 0.54 ± 0.27 ng/μL. This second phase of slower RNA depletion correlates with green rust formation (Figure 3d).

To confirm, that the measured RNA in the solution is not from contamination, a control experiment was performed as described, but no *Saccharomyces cerevisiae* RNA was added. The results reveal that RNA concentrations at $t_{(0)}$ and $t_{(end)}$ in the solution and in the chimney were all below the detection limit of the Qubit Fluorometer (Table S1). This provides evidence, that all detected RNA in the five experimental replicates was from *Saccharomyces cerevisiae*.

Another control experiment with *Saccharomyces cerevisiae* RNA but no chimney confirmed that the RNA depletion in the solution was not due to degradation, but due to chimney growth (Figure 3a). The rate of natural RNA degradation without a chimney was relatively slow and only decreased <10% over the course of the experiment. In contrast, with a chimney, the RNA was depleted ≥99% and was below the detection limit of the Qubit Fluorometer by the end of the experiment (Figure 3b).

No RNA could be extracted from the ferruginous solution without the addition of a phosphate ($1\,M\,Na_2HPO_4$) buffer (Figure 3c),

indicating that the dissolved RNA is likely adsorbed onto iron particles in the solution as described previously (Muto et al., 2017).

3.4 | RNA accumulation in chimneys

When a chimney was present, RNA concentrations decreased 1000-fold in the ferruginous solution compared to the starting concentration (Figure 4a). This contrasts with conditions of a control experiment, where no alkaline fluid was injected, hence no chimney was formed. Here, only a minor decrease in RNA concentration in the iron solution was observed (Figure 3a). At the end of the experiments with a green rust chimney, the concentration of RNA in the chimney (765 ± 79 ng per gram) was significantly higher (two-sided *t*-test: $p = 0.000031$) than the concentration of RNA in the solution at the end of the experiment (20 ± 4 ng per gram) (Figure 4a; Table S2). Without a phosphate extraction buffer, no RNA was extractable from the chimney samples. This indicates that the RNA was complexed with the iron in the chimney, a well-known feature of iron-containing minerals (and clay minerals in general) that bind nucleic acids and reduce their extractability (Muto et al., 2017).
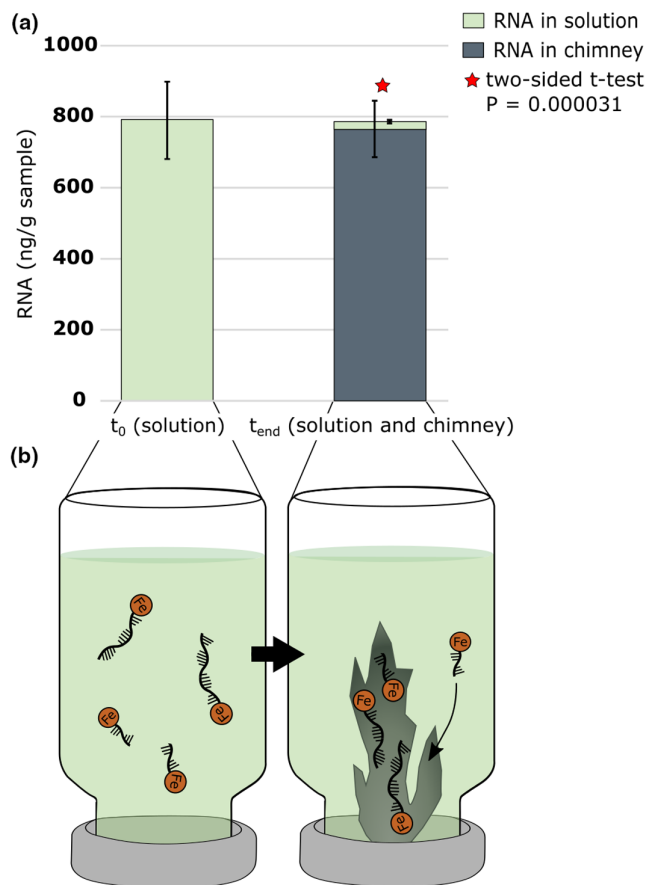
FIGURE 4 Accumulation of RNA in the white and green rust chimneys. (a) Bar charts show the average of RNA in ng/g in the ferruginous solution at the beginning (t_0) and the end (t_{end}) of five experimental replicates (green bar charts). The grey bar chart shows the mean RNA from five different chimneys. RNA data listed in Table S2. Error bars represent standard error of the means. The two-sided t-test was significant with $p = 0.000031$. (b) Schematic drawing of Fe-RNA complexes in the solution getting incorporated into the chimney while it grows. At $t(_{end})$, almost no RNA was detected in the solution, as it was mainly detected in the chimney (a).

4 | DISCUSSION

4.1 | Experimental geochemical conditions in the context of predictions for early Earth

We tested key geochemical aspects of the prebiotic ocean on early Earth, anoxic and ferruginous conditions. It is widely accepted that these seawater conditions were characteristic of the Hadean and Archean (Poulton & Canfield, 2011). Our alkaline vent experiments are based on the prediction, that widespread serpentinization of the oceanic lithosphere was common in prebiotic oceans (Camprubí et al., 2019; Russell, 2018). This probably resulted in venting of high pH fluids at the seafloor, forming alkaline springs when the alkaline fluids came in contact with the ferruginous ocean. We chose pH 3 for the ferruginous solution and pH 13 for the alkaline fluid, since these conditions facilitated

repeatable chimney growth structures and did not impact the overall results.

Our experiments were carried out at 25°C room temperature, which seems justified considering that temperature estimates of the prebiotic ocean are highly uncertain (Altair et al., 2021; Camprubí et al., 2019), ranging from boiling to freezing conditions (Kasting & Ackerman, 1986). Hydrothermal activity can proceed over an even broader range from <10°C to about 407°C (German et al., 2008). Thus, our ambient experimental conditions represent a relatively cool off-ridge environment. We also show that hydrothermal conditions with elevated temperatures are not necessarily required for the formation of green rust chimneys in a ferruginous solution. Relatively mild temperatures are not out of the question in terms of prebiotic ocean conditions, since recent models predict temperatures for some regions of the prebiotic ocean down to as low as 0 to 50°C (Krissansen-Totton et al., 2018). The fact that our green rust chimneys form at 25°C is also beneficial to RNA stability compared to elevated temperatures (Jo et al., 2022).

We were not able to simulate high pressures in the anaerobic chamber. Thus, all experiments were performed at atmospheric pressure, which is relatively low and not representative of the deep sea, where many hydrothermal vents are found (Baker & German, 2004). However, shallow water alkaline vents might have been located near oceanic islands, island arcs or continental shelves, if they existed in the Hadean and Archean, which is highly debatable (Arndt & Nisbet, 2012). Nonetheless, many of the earliest fossils known today are located in shallow water settings, like the 3.4 Ga Strelley Pool Formation in the Pilbara Craton of Western Australia (Sugitani et al., 2015). Moreover, modern examples of such shallow serpentinite-hosted vents today are the Strytan Hydrothermal Field in Iceland or the Prony Hydrothermal Field in New Caledonia (Quéméneur et al., 2014), showing the possibility of hosting complex biological communities. In conclusion, water depth and pressure mimicked in our experiments could represent shallow water vents (Barge & Price, 2022), that hold some of the earliest signs of life in the fossil record according to Sugitani et al. (2015), but the results need to be reviewed with caution. The recent study by Barge and Price (2022) mentions the growing importance of shallow-sea alkaline hydrothermal vents and their possibility to facilitate life-forming reactions.

4.2 | Assessing oxidation of the chimneys

It is known that green rust oxidizes quite fast upon air exposure (Usman et al., 2018). Therefore, we carefully assessed the possibility for oxidation in our experiments. Oxygen exposure during the alkaline vent experiments ($O_2 < 0.01\%$ of present atmospheric values) and sample transfer (transport in N_2 purged gas tight flasks) was kept at a minimum. We acknowledge, that some oxidation might have occurred during the transfer of the chimneys to the microscope. The SEM and elemental analysis indicate effects of oxidation to be minor and resulted in small hematite globules (<10 μm in size) that are likely

the first signs of oxidation (Figure 2a). This likely has to do with SEM measurements being made in a vacuum chamber with no air, and the sample being exposed to air for only a few seconds during transfer. However, when the sample was scanned with the Raman it was not in a vacuum and showed strong signs of oxidation after 20 min where the entire chimney had been oxidized to hematite (Figure S2). When the green rust chimney was measured with the Raman within 1 or 2 min, the characteristic Raman bands at 419 and 506 cm^{-1} for green rust (Usman et al., 2018) were observed (Figure 2c). Therefore, our results indicate that we are forming green rust in the anaerobic chamber that quickly oxidizes to hematite under the Raman. However, it is possible to obtain the green rust spectra with the Raman when measuring quickly after transfer from the gas tight anoxic flask. As expected, the oxidation in air changes the green rust to hematite relatively quickly.

4.3 | Mineralogy and morphology of the chimneys

Evidence for injection-growth experiments under ferruginous conditions forming white and green rust, is scarce. For this reason, we simulated iron hydroxide chimneys in an anaerobic chamber. The first white phase that precipitates in our alkaline vent experiments is probably $Fe(OH)_2$ sometimes referred to as amakinite (Trolard et al., 2022). It shows the typical white color for ferrous iron hydroxide (Lutz et al., 1994) and turns green when it comes in contact with the ferruginous solution in less than 5 min (Figure 3e), indicating oxidation and green rust formation (Barge et al., 2015; Trolard et al., 2007). Difficulties arose, when we attempted to investigate the white rust phase, because of its quick transformation into green rust during the AHV experiment and the lacking ability to dry this highly metastable phase in order to microscopically analyze it. A pure white rust chimney collapses immediately when we attempted to remove the ferruginous solution with a syringe. It was only after the phase transition to green rust that the chimney increases in stability and the solution can be removed with no problem. Similarities in other studies point to this first precipitated phase being ferrous hydroxide $Fe(OH)_2$. Stone et al. (2005) also performed chemical garden chimney growth experiments across pH gradients in ferruginous solutions, and identified the oxidized precipitate of iron in aqueous solutions as ferrous hydroxide $Fe(OH)_2$, namely "white rust". Trolard et al. (2022) describe the precipitation of ferrous hydroxide after mixing a Fe(II) salt solution with sodium hydroxide. Barge et al. (2015) identify the first precipitates in a green rust forming experiment as white rust (iron hydroxide) as well. White rust forms by oxidation and partial hydrolysis of dissolved Fe^{2+} (Trolard et al., 2007), which is the process described in our experiments.

Green rust showed a higher stability than white rust under anoxic conditions, which allowed us to dry the chimneys and prepare them for measurements. Since $FeCl_2*4H_2O$ was used as a salt for the ferruginous solution, chloride-containing green rust GR1-Cl was formed out of the precursor phase white rust (Duval et al., 2019;

Trolard et al., 2022). Depending on the intercalated anion in the double layer hydroxide structure, different varieties of green rust are possible, Cl^-, CO_3^{2-} or SO_4^{2-} green rust for example (Russell, 2018; Trolard et al., 2007). The hexagonal and tabular morphologies of the crystals (Figure 2a) are a typical indicator for green rust as well (Duval et al., 2019; Trolard et al., 2007; Usman et al., 2018). Our chimneys show very similar Raman bands to Usman et al. (2018) and Cambier et al. (2014) that are albeit slightly shifted to 419 and 506 cm^{-1} (Figure 2c).

Chimney morphologies like ours (but with varying chemistries) have been formed in different AHV experiments in the past (Barge et al., 2015, 2020; Burcar et al., 2015; White et al., 2015). The spontaneously formed chemical gardens are made out of vertically oriented chimneys with high internal surface areas that act as flow-through chemical reactors composed of inorganic membranes (Barge et al., 2020). The mainly vertical formation of the chimney structures might be due to fluid buoyancy effects, suggesting the injected sodium hydroxide was less dense than the iron-rich solution (Barge et al., 2012). Experiments performed in microgravity showed no preferred chimney growth orientation (Barge et al., 2012). The injection of 7 mL 0.2 M NaOH with pH 13 had no measurable effect on the pH of the ferruginous solution, which was at pH 3 for the entire duration of the experiment. This could either indicate that the OH$^-$ was being consumed completely by the green rust chimney structure as it grew over time, or the amount of NaOH pumped into the ferruginous solution was simply too small to overcome its buffering capacity.

4.4 | An alternative RNA concentration mechanism compared to wet-dry cycles based on RNA-iron complexation

Generally, adsorption of RNA onto mineral surfaces is a known process particularly in the emergence of life context (Altair et al., 2021; Biondi et al., 2017; Cleaves II et al., 2011; Mizuuchi et al., 2019; Muto et al., 2017; Pedreira-Segade et al., 2016). Especially phyllosilicates are known to adsorb nucleotides, like Fe-Mg-rich swelling clays (Pedreira-Segade et al., 2016). The observation that divalent cations like Mg^{2+} or Fe^{2+} stabilize nucleotides better than monovalent cations (Bowman et al., 2012), supports the importance of the iron-rich mineral green rust. Furthermore, Fe^{2+} can replace Mg^{2+} as the dominant divalent cation during key catalytic RNA functions (Athavale et al., 2012; Bray et al., 2018), indicating that Fe^{2+} was a potential important chelator of RNA in the ferruginous prebiotic oceans.

A fundamental question addressed in our AHV study is the mechanism of RNA sequestration into the chimney. Our results show that RNA is already complexed with Fe^{2+} in the ferruginous solution and that it is concentrated in the chimney as it grows over time (Figure 4b). The iron in solution facilitates the sequestration of RNA into the mineral structure as the chimney precipitates out of solution across the pH gradient. This is evident, because no RNA

was extractable from the ferruginous solution without a phosphate buffer (Figure 3c), showing that the RNA is complexed to iron in the solution.

Wet-dry cycles in warm little ponds are often invoked as possible concentration sites for nucleic acids on an early Earth's surface (Damer & Deamer, 2020; Darwin, 1871; Pearce et al., 2017) that can lead to polymerization (Pearce et al., 2017). Our findings offer an additional plausible concentration mechanism of RNA that does not depend on wet-dry cycles. This is facilitated instead by white and green rust low-temperature alkaline vents. To our knowledge, this is also the first experimental evidence that RNA-iron complexation facilitates the concentration of RNA in an AHV. This opens up the possibility that RNA oligo- and/or polymerization could also occur in AHVs under these conditions.

4.5 | RNA accumulation dynamics in the green rust chimney

RNA accumulation inside the chimney could either be correlated to the height of the chimney, where the amount of RNA in solution decreases as the chimney grows, or the phase transition of white to green rust. RNA seems to bind faster to the initial white rust phase in the first 4 min compared to green rust that forms several minutes later (Videos S1 and S2). The first 10 min of the experimental replicates 3, 4 and 5 reveal, that the highest depletion of RNA in solution takes place in the first 4 min, where the average RNA concentration drops from 4.82 ± 0.30 to 1.02 ± 0.32 ng/µL (Figure 3d). In this period, the chimney growth rate is also the fastest.

In the control experiment without a chimney, the natural RNA degradation (Figure 3a) was minimal, which does not explain the depletion of RNA in the ferruginous solution in the presence of a chimney. Instead, the RNA gets depleted rapidly if a chimney is present (Figure 3b). Thus, the white and green rust chimneys offer a favorable and highly reactive location for the RNA to accumulate. This is evident, when considering that at the end of the experiments higher concentrations of RNA were extracted from the dried green rust chimney compared to the surrounding solution at $t_{(end)}$. Therefore, the RNA is likely moving from the ferruginous solution into the chimney over time and as it grows. The mean of recovered total RNA at $t_{(0)}$ and $t_{(end)}$ is highly similar, showing that there appears to be a mass balance between the RNA concentration at $t_{(0)}$ in the solution and at $t_{(end)}$ in the chimney (Figure 4a).

The variability in RNA concentrations between experiments is likely due to several other factors that introduce variability into the setup such as (1) variation in the chimney growth rate, (2) variation in chimney morphologies, (3) variation in the oxygen concentration in the chamber between 20 and 100 ppm which affects the rate and amount of green rust that forms, and (4) variable amounts of chimney material often get lost to solution in fluid jets or during sample transfer. Nevertheless, the variation is relatively low, indicating that our results are reproducible (Figure 3b; Table S1).

4.6 | Implications for RNA world theories

The RNA world receives strong support from the discovery that all proteins in living organisms are synthesized by a ribozyme at the center of the ribosome (Cech, 2000). Ribozymes, which are enzymes, whose catalytic centers are entirely made of RNA (Scott, 2007), may be the next higher functional building block on the way to a living organism. Ribozymes, which can cleave, join and replicate, are key components for protein synthesis, since they are part of the ribosomes of cellular organisms (Moelling & Broecker, 2021). Thus, it is believed that ribozymes preceded DNA and proteins during evolution (Moelling & Broecker, 2021). Successful trapping and accumulation of ribozymes at iron hydroxide chimneys in future experiments would not only underline the hypothesis of white rust and green rust as important minerals, but of AHVs in general during the emergence of life. Furthermore, Athavale et al. (2012) highlight the importance of the presence of Fe^{2+} over Mg^{2+} in prebiotic oceans, and how Fe^{2+} enhances the catalytic activities of ribozymes.

We acknowledge, that because our tested RNA came from yeast, it is not an ideal proxy for ribozymes. Because the RNA is derived from a living organism (yeast), our experimental setup is not immediately comparable to a possible RNA world that might have consisted of prebiotic self-replicating RNAs. Our experimental setup is similar to that used by McGlynn et al. (2012) who also used RNA from yeast to test hypotheses surrounding the influence of iron sulfide and iron hydroxide minerals on RNA-complexation and binding dynamics in hydrothermal chimney structures (McGlynn et al., 2012). Using a similar logic, we used yeast RNA as a simplification to study how RNA accumulation can occur in white and green rust chimneys forming under simulated geochemical conditions of the early Earth (ferruginous, anoxic). Despite deriving from a living organism, the yeast RNA shares many biochemical and biophysical properties with ribozymes. For example, yeast RNA and ribozymes should both represent soluble charged biomolecules that would promote binding iron minerals like green rust. However, the shorter strand length of ribozymes and potentially different or lower nucleotide diversity of the ribozymes could affect binding to the white rust and green rust, which should be a focus of future studies to see if the same concentration dynamics seen here for yeast RNA also applies to ribozymes.

5 | OUTLOOK

The mineral green rust has been proposed as one of the key minerals in life's emergence, which underlines the significance of our results that white to green rust transforming chimneys accumulate RNA from a ferruginous solution. No rocks exist on the Earth that are older than 4 Ga, but our experiments indicate that green rust chimneys may have been a feature of the early Earth seafloor at alkaline springs under ferruginous conditions. RNA concentrating

mechanisms may have promoted survival of self-replicating RNAs, that otherwise would be diluted to extremely low concentrations in the early ferruginous oceans during the Hadean and Archaean. In contrast to alkaline vents, wet-dry cycles in warm little ponds are a potential place for concentrating biomolecules at life's emergence. Our study shows that white and green rust composed chimneys accumulate RNA from a ferruginous solution, thereby providing an additional potential mechanism to help solve the "concentration problem" (De Duve, 1991) for RNA in a prebiotic ocean.

CONFLICT OF INTEREST STATEMENT
The authors declare no conflict of interest.

DATA AVAILABILITY STATEMENT
The data that supports the findings of this study are available in the supplementary material of this article.

ORCID
Vanessa Helmbrecht https://orcid.org/0000-0002-7537-3798

REFERENCES
Altair, T., Borges, L. G., Galante, D., & Varela, H. (2021). Experimental approaches for testing the hypothesis of the emergence of life at submarine alkaline vents. *Life, 11*(8), 777.

Arndt, N. T., & Nisbet, E. G. (2012). Processes on the young earth and the habitats of early life. *Annual Review of Earth and Planetary Sciences, 40*(521), 2012–2549.

Arrhenius, G. O. (2003). Crystals and life. *Helvetica Chimica Acta, 86*, 1569–1586.

Athavale, S. S., Petrov, A. S., Hsiao, C., Watkins, D., Prickett, C. D., Gossett, J. J., Lie, L., Bowman, J. C., O'Neill, E., Bernier, C. R., Hud, N. V., Wartell, R. M., Harvey, S. C., & Williams, L. D. (2012). RNA folding and catalysis mediated by iron (II). *PLoS One, 7*(5), e38024.

Baaske, P., Weinert, F. M., Duhr, S., Lemke, K. H., Russell, M. J., & Braun, D. (2007). Extreme accumulation of nucleotides in simulated hydrothermal pore systems. *Proceedings of the National Academy of Sciences of the United States of America, 104*(22), 9346–9351.

Baker, E. T., & German, C. R. (2004). On the global distribution of hydrothermal vent fields. Mid-Ocean ridges: Hydrothermal interactions between the lithosphere and oceans. *Geophysical Monograph Series, 148*, 245–266.

Barge, L. M., Cardoso, S. S., Cartwright, J. H., Cooper, G. J., Cronin, L., De Wit, A., Doloboff, I. J., Escribano, B., Goldstein, R. E., Haudin, F., Jones, D. E. H., Mackay, A. L., Maselko, J., Pagano, J. J., Pantaleone, J., Russell, M. J., Sainz-Díaz, C. I., Steinbock, O., Stone, D. A., … Thomas, N. L. (2015). From chemical gardens to chemobrionics. *Chemical Reviews, 115*(16), 8652–8703.

Barge, L. M., Doloboff, I. J., White, L. M., Stucky, G. D., Russell, M. J., & Kanik, I. (2012). Characterization of iron–phosphate–silicate chemical garden structures. *Langmuir, 28*(8), 3714–3721.

Barge, L. M., Jones, J. P., Pagano, J. J., Martinez, E., & Bescup, J. (2020). Three-dimensional analysis of a simulated prebiotic hydrothermal chimney. *ACS Earth and Space Chemistry, 4*(9), 1663–1669.

Barge, L. M., & Price, R. E. (2022). Diverse geochemical conditions for prebiotic chemistry in shallow-sea alkaline hydrothermal vents. *Nature Geoscience, 15*, 1–6.

Beard, J. S., Frost, B. R., Fryer, P., McCaig, A., Searle, R., Ildefonse, B., Zinin, P., & Sharma, S. K. (2009). Onset and progression of serpentinization and magnetite formation in olivine-rich troctolite from IODP hole U1309D. *Journal of Petrology, 50*(3), 387–403.

Bernal, J. D., Dasgupta, D. T., & Mackay, A. L. (1959). The oxides and hydroxides of iron and their structural interrelationships. *Clay Minerals Bulletin, 4*, 15–30.

Biondi, E., Furukawa, Y., Kawai, J., & Benner, S. A. (2017). Adsorption of RNA on mineral surfaces and mineral precipitates. *Beilstein Journal of Organic Chemistry, 13*(1), 393–404.

Bowman, J. C., Lenz, T. K., Hud, N. V., & Williams, L. D. (2012). Cations in charge: Magnesium ions in RNA folding and catalysis. *Current Opinion in Structural Biology, 22*, 262–272.

Bray, M. S., Lenz, T. K., Haynes, J. W., Bowman, J. C., Petrov, A. S., Reddi, A. R., Hud, N. V., Williams, L. D., & Glass, J. B. (2018). Multiple prebiotic metals mediate translation. *PNAS, 115*(48), 12164–12169.

Burcar, B. T., Barge, L. M., Trail, D., Watson, E. B., Russell, M. J., & McGown, L. B. (2015). RNA oligomerization in laboratory analogues of alkaline hydrothermal vent systems. *Astrobiology, 15*(7), 509–522.

Cambier, S. M., Verreault, D., & Frankel, G. S. (2014). Raman investigation of anodic undermining of coated steel during environmental exposure. *Corrosion, 70*(12), 1219–1229.

Camprubí, E., De Leeuw, J. W., House, C. H., Raulin, F., Russell, M. J., Spang, A., Tirumalai, M. R., & Westall, F. (2019). The emergence of life. *Space Science Reviews, 215*(8), 1–53.

Cech, T. R. (2000). The ribosome is a ribozyme. *Science, 289*(5481), 878–879.

Charlou, J. L., Fouquet, Y., Bougault, H., Donval, J. P., Etoubleau, J., Jean-Baptiste, P., Dapoigny, A., Appriou, P., & Rona, P. A. (1998). Intense CH4 plumes generated by serpentinization of ultramafic rocks at the intersection of the 15° 20′ N fracture zone and the mid-Atlantic ridge. *Geochimica et Cosmochimica Acta, 62*(13), 2323–2333.

Cleaves, H. J., II, Crapster-Pregont, E., Jonsson, C. M., Jonsson, C. L., Sverjensky, D. A., & Hazen, R. A. (2011). The adsorption of short single-stranded DNA oligomers to mineral surfaces. *Chemosphere, 83*(11), 1560–1567.

Damer, B., & Deamer, D. (2020). The hot spring hypothesis for an origin of life. *Astrobiology, 20*(4), 429–452.

Darwin, C. (1871). Darwin correspondence project, "Letter No. 7471".

De Duve, C. (1991). *Blueprint for a cell: The nature and origin of life*.

Drozdovskiy, I., Ligeza, G., Jahoda, P., Franke, M., Lennert, P., Vodnik, P., Payler, S. J., Kaliwoda, M., Pozzobon, R., Massironi, M., Turchi, L., Bessone, L., & Sauro, F. (2020). The PANGAEA mineralogical database. *Data in Brief, 31*, 105985.

Duval, S., Baymann, F., Schoepp-Cothenet, B., Trolard, F., Bourrié, G., Grauby, O., Branscomb, E., Russell, M. J., & Nitschke, W. (2019). Fougerite: The not so simple progenitor of the first cells. *Interface Focus, 9*(6), 20190063.

German, C. R., Bennett, S. A., Connelly, D. P., Evans, A. J., Murton, B. J., Parson, L. M., Prien, R. D., Ramirez-Llodra, E., Jakuba, M., Shank,

T. M., Yoerger, D. R., Baker, E. T., Walker, S. L., & Nakamura, K. (2008). Hydrothermal activity on the southern mid-Atlantic ridge: Tectonically-and volcanically-controlled venting at 4–5 S. *Earth and Planetary Science Letters*, *273*(3–4), 332–344.

Gilbert, W. (1986). Origin of life: The RNA world. *Nature*, *319*(6055), 618.

Halevy, I., Alesker, M., Schuster, E. M., Popovitz-Biro, R., & Feldman, Y. (2017). A key role for green rust in the Precambrian oceans and the genesis of iron formations. *Nature Geoscience*, *10*(2), 135–139.

Heller, R., Duda, J. P., Winkler, M., Reitner, J., & Gizon, L. (2021). Habitability of the early earth: Liquid water under a faint young sun facilitated by strong tidal heating due to a closer moon. *PalZ*, *95*, 1–13.

Jo, T., Tsuri, K., Hirohara, T., & Yamanaka, H. (2022). Warm temperature and alkaline conditions accelerate environmental RNA degradation. *Environmental DNA*, 1–13. https://doi.org/10.1002/edn3.334

Kasting, J. F., & Ackerman, T. P. (1986). Climatic consequences of very high carbon dioxide levels in the Earth's early atmosphere. *Science*, *234*(4782), 1383–1385.

Kelley, D. S., Karson, J. A., Blackman, D. K., Früh-Green, G. L., Butterfield, D. A., Lilley, M. D., Olson, E. J., Schrenk, M. O., Roe, K. K., Lebon, G. T., & Rivizzigno, P. (2001). An off-axis hydrothermal vent field near the mid-Atlantic ridge at 30 N. *Nature*, *412*(6843), 145–149.

Klein, F., Bach, W., & McCollom, T. M. (2013). Compositional controls on hydrogen generation during serpentinization of ultramafic rocks. *Lithos*, *178*, 55–69.

Krissansen-Totton, J., Arney, G. N., & Catling, D. C. (2018). Constraining the climate and ocean pH of the early earth with a geological carbon cycle model. *Proceedings of the National Academy of Sciences of the United States of America*, *115*(16), 4105–4110.

Lafuente, B., Downs, R. T., Yang, H., Stone, N., Armbruster, T., & Danisi, R. M. (2015). *Highlights in mineralogical crystallography* (pp. 1–30). W. De Gruyter.

Lutz, H. D., Möller, H., & Schmidt, M. (1994). Lattice vibration spectra. Part LXXXII. Brucite-type hydroxides $M(OH)_2$ (M = Ca, Mn, Co, Fe, Cd)—IR and Raman spectra, neutron diffraction of $Fe(OH)_2$. *Journal of Molecular Structure*, *328*, 121–132.

Martin, W., Baross, J., Kelley, D., & Russell, M. J. (2008). Hydrothermal vents and the origin of life. *Nature Reviews Microbiology*, *6*(11), 805–814.

Martin, W., & Russell, M. J. (2003). On the origins of cells: A hypothesis for the evolutionary transitions from abiotic geochemistry to chemoautotrophic prokaryotes, and from prokaryotes to nucleated cells. *Philosophical Transactions of the Royal Society of London. Series B: Biological Sciences*, *358*(1429), 59–85.

Mast, C. B., & Braun, D. (2010). Thermal trap for DNA replication. *Physical Review Letters*, *104*(18), 188102.

McGlynn, S. E., Kanik, I., & Russell, M. J. (2012). Peptide and RNA contributions to iron–Sulphur chemical gardens as life's first inorganic compartments, catalysts, capacitors and condensers. *Philosophical Transactions of the Royal Society A: Mathematical, Physical and Engineering Sciences*, *370*(1969), 3007–3022.

Mizuuchi, R., Blokhuis, A., Vincent, L., Nghe, P., Lehman, N., & Baum, D. (2019). Mineral surfaces select for longer RNA molecules. *Chemical Communications*, *55*(14), 2090–2093.

Moelling, K., & Broecker, F. (2021). Viroids and the origin of life. *International Journal of Molecular Sciences*, *22*(7), 3476.

Mojzsis, S. J., Harrison, T. M., & Pidgeon, R. T. (2001). Oxygen-isotope evidence from ancient zircons for liquid water at the Earth's surface 4,300 Myr ago. *Nature*, *409*(6817), 178–181.

Muto, H., Takaki, Y., Hirai, M., Mino, S., Sawayama, S., Takai, K., & Nakagawa, S. (2017). A simple and efficient RNA extraction method from Deep-Sea hydrothermal vent chimney structures. *Microbes and Environments*, *32*, 330–335.

Orsi, W. D., Vuillemin, A., Coskun, Ö. K., Rodriguez, P., Oertel, Y., Niggemann, J., Mohrholz, V., & Gomez-Saez, G. V. (2022). Carbon assimilating fungi from surface ocean to subseafloor revealed by coupled phylogenetic and stable isotope analysis. *The ISME Journal*, *16*(5), 1245–1261.

Pearce, K. D. B., Pudritz, R. E., Semenov, D. A., & Henning, T. K. (2017). Origin of the RNA world: The fate of nucleobases in warm little ponds. *Proceedings of the National Academy of Sciences of the United States of America*, *114*(43), 11327–11332.

Pedreira-Segade, U., Feuillie, C., Pelletier, M., Michot, L. J., & Daniel, I. (2016). Adsorption of nucleotides onto ferromagnesian phyllosilicates: Significance for the origin of life. *Geochimica et Cosmochimica Acta*, *176*, 81–95.

Poulton, S. W., & Canfield, D. E. (2011). Ferruginous conditions: A dominant feature of the ocean through Earth's history. *Elements*, *7*(2), 107–112.

Preiner, M., Asche, S., Becker, S., Betts, H. C., Boniface, A., Camprubi, E., Chandru, K., Erastova, V., Garg, S. G., Khawaja, N., Kostyrka, G., Machné, R., Moggioli, G., Muchowska, K. B., Neukirchen, S., Peter, B., Pichlhöfer, E., Radványi, Á., Rossetto, D., … Xavier, J. C. (2020). The future of origin of life research: Bridging decades-old divisions. *Life*, *10*(3), 20.

Quéméneur, M., Bes, M., Postec, A., Mei, N., Hamelin, J., Monnin, C., Chavagnac, V., Payri, C., Pelletier, B., Guentas-Dombrowski, L., Gérard, M., Pisapia, C., Gérard, E., Ménez, B., Ollivier, B., & Erauso, G. (2014). Spatial distribution of microbial communities in the shallow submarine alkaline hydrothermal field of the Prony Bay, New Caledonia. *Environmental Microbiology Reports*, *6*(6), 665–674.

Rouillard, J., García-Ruiz, J. M., Gong, J., & Van Zuilen, M. A. (2018). A morphogram for silica-witherite biomorphs and its application to microfossil identification in the early earth rock record. *Geobiology*, *16*(3), 279–296.

Russell, M. J. (2018). Green rust: The simple organizing 'seed'of all life? *Life*, *8*(3), 35.

Russell, M. J., Nitschke, W., & Branscomb, E. (2013). The inevitable journey to being. *Philosophical Transactions of the Royal Society B: Biological Sciences*, *368*(1622), 20120254.

Scott, W. G. (2007). Ribozymes. *Current Opinion in Structural Biology*, *17*(3), 280–286.

Stone, D. A., Lewellyn, B., Baygents, J. C., & Goldstein, R. E. (2005). Precipitative growth templated by a fluid jet. *Langmuir*, *21*(24), 10916–10919.

Sugitani, K., Mimura, K., Takeuchi, M., Yamaguchi, T., Suzuki, K., Senda, R., Asahara, Y., & Van Kranendonk, M. J. (2015). A Paleoarchean coastal hydrothermal field inhabited by diverse microbial communities: The Strelley Pool formation, Pilbara craton. *Western Australia. Geobiology*, *13*(6), 522–545.

Trolard, F., Bourrié, G., Abdelmoula, M., Refait, P., & Feder, F. (2007). Fougerite, a new mineral of the pyroaurite-iowaite group: Description and crystal structure. *Clays and Clay Minerals*, *55*(3), 323–334.

Trolard, F., Duval, S., Nitschke, W., Ménez, B., Pisapia, C., Nacib, J. B., Andréani, M., & Bourrié, G. (2022). Mineralogy, geochemistry and occurrences of fougerite in a modern hydrothermal system and its implications for the origin of life. *Earth-Science Reviews*, *225*, 103910.

Usman, M., Byrne, J. M., Chaudhary, A., Orsetti, S., Hanna, K., Ruby, C., Kappler, A., & Haderlein, S. B. (2018). Magnetite and green rust: Synthesis, properties, and environmental applications of mixed-valent iron minerals. *Chemical Reviews*, *118*(7), 3251–3304.

White, L. M., Bhartia, R., Stucky, G. D., Kanik, I., & Russell, M. J. (2015). Mackinawite and greigite in ancient alkaline hydrothermal chimneys: Identifying potential key catalysts for emergent life. *Earth and Planetary Science Letters*, *430*, 105–114.

White, L. M., Shibuya, T., Vance, S. D., Christensen, L. E., Bhartia, R., Kidd, R., Hoffmann, A., Stucky, G. D., Kanik, I., & Russell, M. J. (2020). Simulating serpentinization as it could apply to the emergence of life using the JPL hydrothermal reactor. *Astrobiology*, *20*(3), 307–326.

SUPPORTING INFORMATION

Additional supporting information can be found online in the Supporting Information section at the end of this article.